

Visibility Monitoring using Mobile Phones

Sameera Poduri, Anoop Nimkar and Gaurav S. Sukhatme

Department of Computer Science,
University of Southern California
{sameera, nimkar, gaurav}@usc.edu

ABSTRACT

Airborne particulate matter is a serious threat to both our health and the environment. It is also the primary cause for visibility degradation in urban metropolitan areas. We present the design, implementation, and evaluation of an optical technique to measure visibility using commodity cameras and other sensors commonly found on mobile phones. The user takes a picture of the sky which is tagged with location, orientation, and time data and transferred to a back-end server. Visibility is estimated by first calibrating the image radiometrically and then comparing the intensity with a physics-based model of sky luminance. We describe the challenges for development of the system on the HTC G1 phone running the Android OS. We study the sensitivity of the technique to error in the accelerometers and magnetometers. Results from images gathered in Phoenix, Arizona and the Los Angeles basin compare favorably to air quality data published by the US Environmental Protection Agency.

1. INTRODUCTION

Atmospheric visibility refers to the clarity with which distant objects are perceived. It is important as a measure of air quality, driving safety, and for tourism. Without the effects of manmade air pollution, the natural visual range would be nearly 140 miles in western USA and 90 miles in the eastern areas [1]. Today the visibility has decreased to 35-90 miles in the west and 15-25 miles in the east. The atmospheric pollutants that most often affect visibility exist as haze aerosols which are tiny particles ($10\mu\text{m}$ and smaller) dispersed in air that scatter sunlight, imparting a distinctive gray hue to the sky. The suspended particles may originate as emissions from natural sources (e.g., sea salt entrainment and wind-blown dust) or from manmade sources (e.g., automobile exhaust and mining activities). This particulate matter or PM is cited as a key reason for heart and lung problems, especially in metropolitan areas such as Los Angeles [4]. Recent studies also show that particulate matter enhances global warming [13]. Atmospheric visibility is a measure of particulate matter concentration [11]. The United States' Environment Protection Agency (EPA) initiated the Interagency Monitoring of Protected Environments (IMPROVE) in 1985 with to monitor air quality and visibility in 157 national parks

and wilderness regions across the country. In 1999, the Regional Haze Regulation was promulgated which mandates improvement of atmospheric visibility.

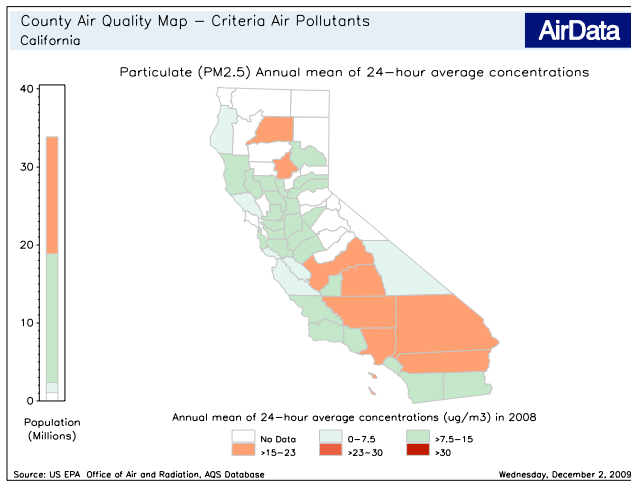


Figure 1: Los Angeles is ranked as one of the most polluted cities in the country in terms of year-round particle pollution

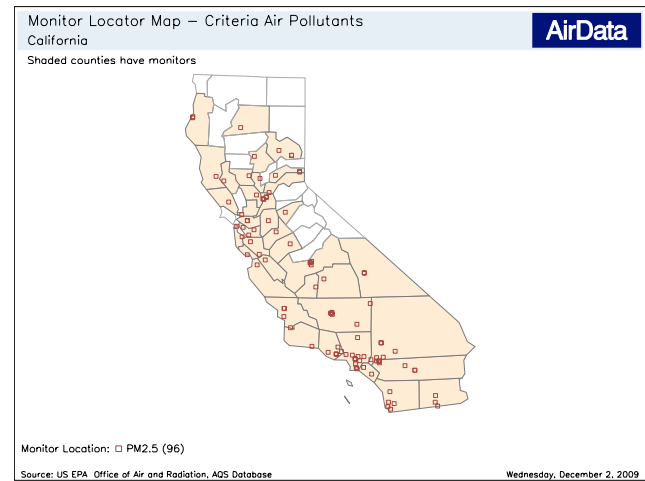
While monitoring air visibility is important for our health as well as the environment, current monitoring stations are very sparsely deployed (figure 2). Visibility is typically measured using human observers, optical instruments such as photometers and transmissometers or chemical sensors such as integrating nephelometers. While the human observer method suffers due to subjectivity, optical and chemical measurement is very precise but expensive and requires maintenance. In several developing countries around the world, there is little or no monitoring infrastructure available.

Our goal is to develop an air visibility sensing system that uses off-the-shelf sensors and can be easily deployed to be used by a large number of people. This will enable large-scale sensing of visibility and augment existing instrumentation that is precise but expensive and sparse. We propose to use phones for two reasons - 1) phones have proliferated all over the world and can potentially allow massive sensing coverage 2) most high end phones are equipped with cameras and other sophisticated sensors that can be used to measure visibility and 3) having a human in the loop can help intelligent data collection and also to gather data where it matters.

Our application works as follows. The user starts an ap-



(a)



(b)

Figure 2: (a) Average particulate matter concentration in California. The orange regions are above the air quality standard stipulated by EPA. (b) Monitoring stations are sparsely deployed. The counties in white have no monitoring stations.

plication on his phone, points the phone to the sky and takes a picture. The application tags the image with accelerometer, magnetometer, date and time information and stores it on the phone. It uses the GPS and time information to compute current solar position, appends this to the tag file, and sends it along with the image to a backend server. The solar and camera orientation data is used to compute an analytic model of the sky as a function of the atmospheric visibility. By comparing this with the intensity profile of the image, we estimate visibility. If the user prefers, the application can also transfer his GPS coordinates to the backend server so that the visibility information is displayed on a map to be shared with other users.

The main contributions of this work are as follows.

- Design of a visibility estimation algorithm that takes as input an image of the sky, orientation of the camera and solar orientation
- Design and implementation of the system to on HTC G1 phones taking into account privacy and efficiency factors
- Evaluation of the system using images from 3 different sources and analysis of effect of sensor noise

The paper is organized as follows. The next section defines metrics for atmospheric visibility and gives an overview of the common methods of measuring it and its relation to air quality. Section 3 presents the architecture and design of the system and its implementation on HTC G1 smartphone. The sky luminance model, radiometric calibration technique and visibility estimation algorithm are described in section 4. This is followed by experimental results including sensitivity analysis in section 5.1. We place the work in context by

describing related research in section 6 and conclude with a discussion in section 7.

2. VISIBILITY

Visibility varies because light gets scattered and absorbed by particles and gases in the atmosphere. According to the EPA, particulate matter pollution is the major cause of reduced visibility (haze) in parts of the United States. Because particles typically scatter more uniformly than molecules for all wavelengths, haze causes a whitening of the sky. The particles can come from many sources - industrial and vehicular emissions, volcanic eruptions, forest fires, cosmic bombardment, the oceans, etc. A commonly used measure of atmospheric visibility is the meteorological range R_m which is the distance under daylight conditions at which the apparent contrast between a black target and its background (horizon sky) becomes equal to a threshold constant of an observer, and it roughly corresponds to the distance to the most distant discernible geographic feature [11]. Koschmieder derived a formula that relates the meteorological range to the aerosol extinction coefficient β .

$$R_m = \frac{3912}{\beta(Mm^{-1})}$$

The formula shows that visibility closely correlates with aerosol load and it is therefore a good indicator for the air quality.

In atmospheric sciences literature, another metric called turbidity is used. Turbidity is a measure of the fraction of light scattering due to haze as opposed to molecules [11]. Formally, turbidity T is defined as the ratio of the optical thickness of a path in the haze atmosphere (haze particles and molecules) to the optical thickness of the path in atmosphere with the molecules alone:

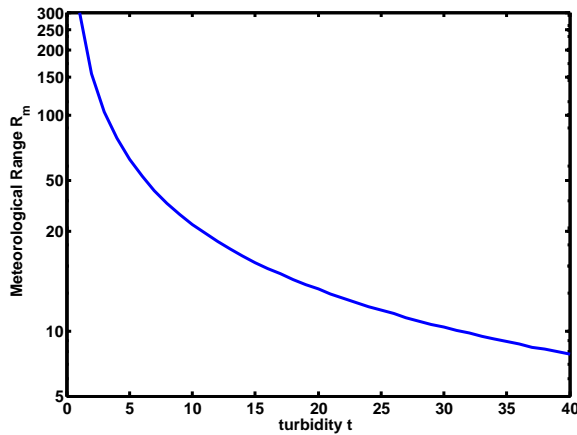


Figure 3: Relation between turbidity and meteorological range in km

$$T = \frac{t_m + t_h}{t_m}$$

where t_m is the vertical optical thickness of the molecular atmosphere, and t_h is the vertical optical thickness of the haze atmosphere. Optical thickness t for a path of length x is defined in terms of the extinction coefficient β as follows

$$t = \int_0^x \beta(x) dx$$

Strictly speaking, visibility is only defined for a path and not for a region. But if the region is homogenous, we can define its visibility as that of a random path. Generally horizontal paths are considered homogenous and vertical paths are least homogenous. In fact, the aerosol concentration rapidly decreases in the vertical direction. Most of the aerosol particles exist in the region 10 – 20 km about the surface of earth. Turbidity and meteorological range are closely related as shown in figure 3

In our work, we estimate turbidity directly using models of sky appearance.

3. SYSTEM DESIGN

In this section, we present the design and implementation of the visibility sensing system. Figure 4 shows the high level architecture. The user gathers a picture that gets automatically tagged with relevant sensor data and transmitted to a backend server which processes the data to estimate visibility and returns a value of turbidity to the user. Based on the privacy preference of the user, the image, its location and turbidity value are displayed on a publicly accessible map and stored onto a database for future analysis.

Our design is based on the following considerations.

- **Privacy:** The visibility estimation algorithm is based on potentially sensitive information such as location

and images. To ensure user privacy, we process the data such that the user is anonymous with respect to the information that leaves the phone. User’s GPS coordinates are used to compute solar position on the phone which is communicated to the backend server without the GPS data. Similarly, the image is cropped and only the segment that contains the sky pixels is shared. However, the user has the option of sharing complete information which can be useful for large-scale monitoring and analysis.

- **Communication cost:** In the default usage mode, the data transfer is initiated immediately after data logging assuming that the phone is connected to the internet. However, we provide an option to delay the transfer until a preferred internet connection is available.
- **No blocking:** After data is transferred, the response from the server may take a few minutes. During this time, the visibility application does not block the phone. Instead, it switches into a background mode where it waits for a response and frees the phone for other applications. On receiving a response it displays it as a notification.
- **Aiding data collection:** Sensors on the phone can guide data collection so that the data is well-suited for the estimation algorithm. We use the phone’s orientation sensors to help the user hold the phone parallel to the ground (without roll) as that yields best results. Similarly, we deactivate the camera button if the zenith angle is more than 100° as we are only interested in images of the sky.
- **Human in the loop:** Several computer vision problems that are extremely challenging to automate are trivially solved by a human. In our system, segmenting sky pixels in an arbitrary image is one such problem. When the user captures an image, we ask him to select a part of the image that is sky. By exploiting the participatory nature of our paradigm, we can build a system that is robust and efficient.
- **Energy efficiency:** The sensors that consume most energy on our system are the GPS and camera. Of these, the GPS is not essential because very coarse, city-scale, localization is sufficient for visibility estimation. The user can turn off GPS in the application making it use either cell tower ID based locations or the last recorded GPS locations.

We will now describe the details of our implementation on the HTC G1 smartphone.

3.1 Hardware

Current high-end mobile phones (such as the iPhone, HTC G1, Nokia N97, BlackBerry, etc) are embedded with cameras, accelerometers, GPS sensors and in some cases, even

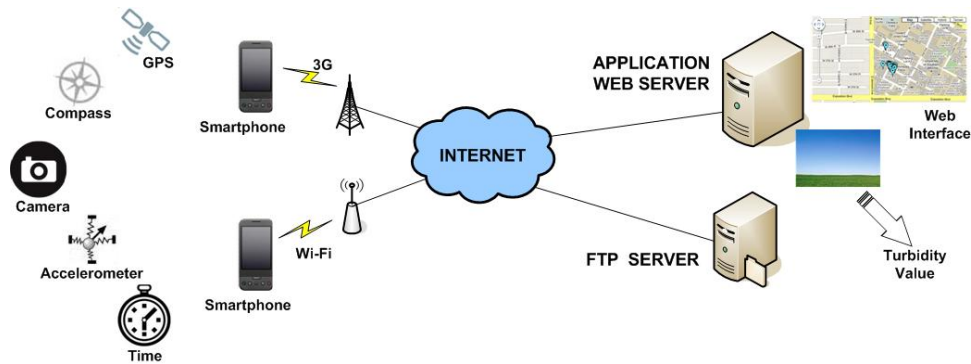


Figure 4: Overview of the system

magnetometers. We chose the HTC G1 phone because it can sense 3D orientation and is easily programmable.

HTC G1 runs Android OS that provides an open SDK and APIs to program sensors. Android is a software stack for different mobile devices that includes the operating system, middleware and application level. Android runs linux kernel and applications are developed in Java to support standard Java APIs as well as libraries for Android specific APIs. The phone has significant computational capability with a 528Mhz processor, 64 MB internal RAM and 128 MB internal ROM for OS and applications. With this processing power, our on-phone computation of solar position is almost instantaneous. The phone has a 1GB MicroSD card where the images taken from camera along with their tags are stored.

The phone is embedded with a 3.1 megapixel camera with a dedicated camera button. It supports JPG, BMP, PNG, and GIF formats. We use RGB format to store color information. The camera does not allow optical zooming which means that all images from a phone have a fixed focal length, thus allowing a one-time calibration. The Android orientation API combines information from a 3-axis magnetic sensor and a 3-axis accelerometer to report the 3D orientation of the phone. It uses a dynamic offset estimation algorithm to compensate for the local magnetic field. We found that in spite of this, there is a significant error in the azimuth values (figure 16). The GPS data is highly accurate (-160 dBm tracking sensitivity) for our purpose.

The backend system consists of FTP and HTTP servers running on a standard desktop that runs MATLAB and communicates with the phone through internet.

3.2 Software Design

Figure 5 shows screenshots of the phone application built on Android 1.5SDK. It begins with a splash screen with options to edit settings or capture an image. On the settings screen the user can choose his internet tagging, privacy and file transfer settings. Turning on the internet tagging option causes the application to tag the image with additional data such as weather information obtained from the internet.

Such information will be useful for further study of visibility conditions. As mentioned earlier, the file transfer option controls whether sensor data will be automatically transferred to the server or stored on the phone and transferred later when the user clicks the 'Transfer files' button. This facility is useful if either the phone does not have 3G capability or if the user prefers to wait for a cheaper WiFi connection. Turning on the privacy filter will prevent GPS data being transferred to the server. If it is off, the GPS data is used to archive the sensor data and display it on a publicly accessible map. When the user clicks the start button, the image capture screen with the camera preview appears. On this screen, the azimuth and zenith angles are shown in green if the roll is less than 5° , i.e., the phone is parallel to the ground. If not, the angles appear in red. If the angles are in green, the user can capture an image by pressing the camera button. The image is saved and displayed on the screen and the user is prompted to choose two points on the image such that the rectangle formed with those points as a diagonal contains only sky pixels. The image is cropped to this box and sent to the server along with a separate tag file containing orientation, date, time, and solar position which is computed on the phone (as described in the next subsection). Files are transferred over standard FTP protocol in which client program runs on phone and FTP server process runs on the backend server. While the orientation data is stored at the time of image capture, the GPS sensor is invoked as soon as the application starts since it can take a few seconds to locate satellites. After segmenting the sky portion of the image, the user can also provide additional information about cloud cover and the apparent visibility. This information will be useful in studying the performance of the system. After this step, the application switches to a background mode where it listens for a message from the backend server. The resulting turbidity estimate is displayed as a notification along with time of image capture.

Figure 6 shows the flow of information and the computations performed on the phone and the backend server. On the phone end, we use location and time information to compute the solar azimuth and elevation angles using the algo-

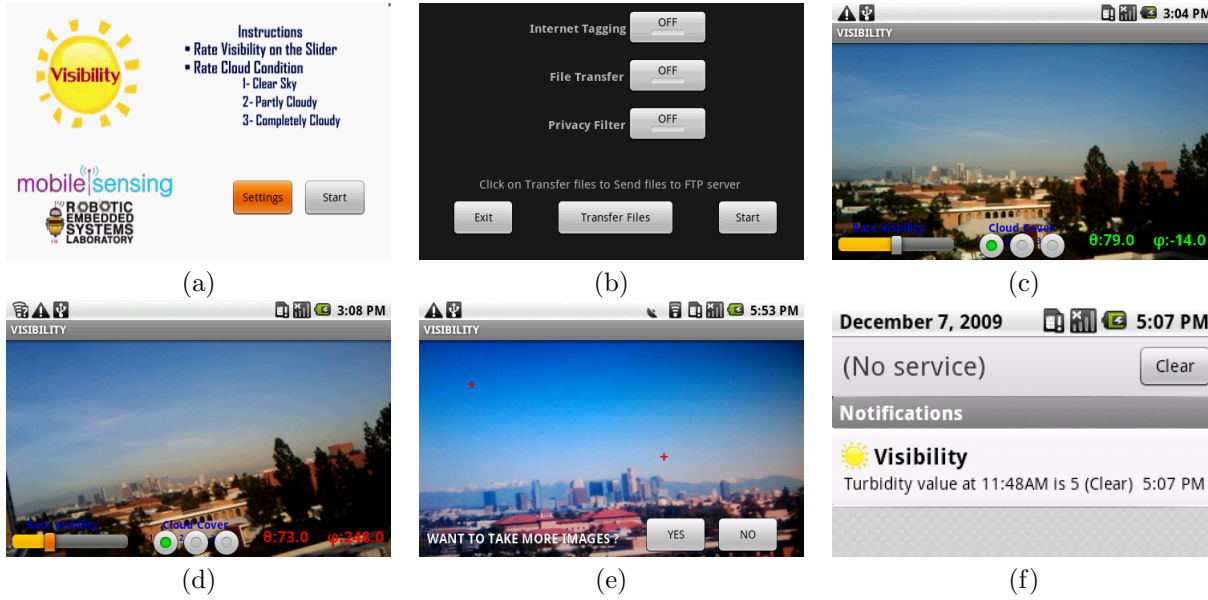


Figure 5: The Visibility application for Android OS. (a) startup screen with options to view/edit settings and start taking the picture. (b) settings for communication and privacy. If internet tagging is turned on, the application will gather weather data. File transfer option allows the user to choose between transferring the image immediately or at a later more convenient time. Privacy filter controls whether the user's GPS data is communicated. (c) Camera preview. The azimuth and zenith angles are displayed in green when the roll is $< 5^\circ$ and red (d) otherwise. (e) The user chooses a portion of sky for processing. Clicking the camera button at this point stores the image along with orientation data. (f) The computed turbidity value is returned as a notification

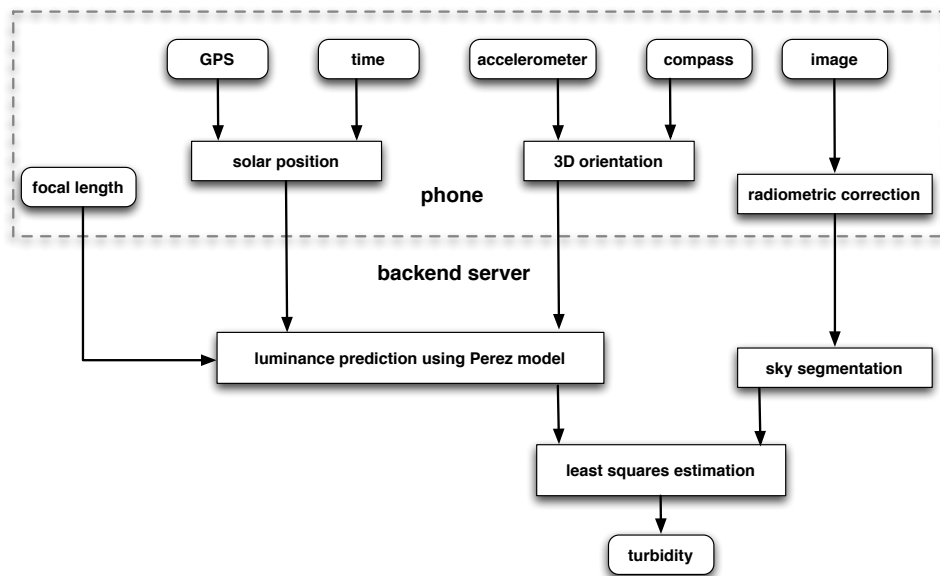


Figure 6: System Architecture

rithm described in [16]. The 3D orientation computation is performed by Android's orientation API.

The backend server runs Perl scripts that are triggered by the phone through HTTP requests. These scripts initiate image processing which includes radiometric correction and computation of image luminance. This is implemented using MATLAB. The camera orientation and solar orientation data are used to compute the analytical model of sky luminance. This is followed by an optimization step to estimate the visibility. The analytical model also uses the focal length information which can usually be obtained from the phone. The resulting visibility value is sent back to the phone as a response to the HTTP request. If the privacy filter is off, then the image along with visibility value is sent to a web server which displays them on a map (figure 7).

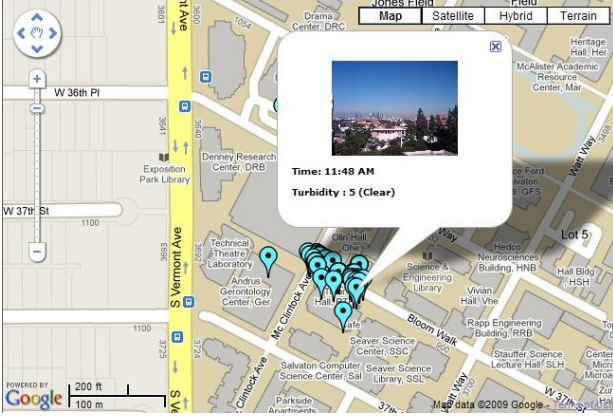


Figure 7: Images and the visibility estimates are displayed on a publicly accessible map.

4. VISIBILITY ESTIMATION

In this section, we describe the details of the analytical sky model, radiometric calibration and visibility estimation algorithm. The method is based on [9] where the sky luminance model is used to calibrate the geometric parameters of the camera assuming clear sky images. In our case, the focal length and orientation of camera are known and we seek to estimate the turbidity of images.

4.1 Sky Luminance

Several physical as well as empirical models for the sky luminance have been proposed [8]. Of these, the model proposed by Perez et al [12] is shown to work well for different weather conditions. It is a generalization of the CIE standard clear sky formula. The luminance of a sky element is given by

$$L(\theta_p, \gamma_p) = L_0 \frac{f(\theta_p, \gamma_p, t)}{f(0, \theta_s)} \quad (1)$$

where θ_p is the zenith of the sky element, γ_p is the angle between the sky element and the sun, and θ_s is the zenith of

the sun. We call f the scaled luminance as it captures the ratio of true luminance to zenith luminance. It is defined as follows.

$$f(\theta_p, \gamma_p, t) = (1+a \cdot e^{(b/\cos(\theta_p))})(1+c \cdot e^{(d \cdot \cos(\gamma_p)+e \cdot \cos^2(\gamma_p)}) \quad (2)$$

where a, b, c, d , and e are adjustable coefficients. Each of the parameters has a specific physical effect on the sky distribution and with different values they can capture a wide variety of sky conditions. An empirical model of the parameters in terms of turbidity t has been proposed [14]

$$\begin{bmatrix} a \\ b \\ c \\ d \\ e \end{bmatrix} = \begin{bmatrix} 0.1787 & 1.4630 \\ -0.3554 & 0.4275 \\ -0.0227 & 5.3251 \\ 0.1206 & -2.5771 \\ -0.0670 & 0.3703 \end{bmatrix} \begin{bmatrix} t \\ 1 \end{bmatrix}$$

Figure 8 shows the variation in the scaled luminance ratio (f) as the value of turbidity changes. There is a significant change in the shape of the surface and this can be used to estimate turbidity.

Equation 2 can be expressed in terms of the pixel coordinates as shown in [9]. We reproduce the equations here for clarity.

$$\theta_p = \arccos\left(\frac{v_p \sin(\theta_c) + f_c \cos(\theta_c)}{\sqrt{f_c^2 + u_p^2 + v_p^2}}\right)$$

$$\phi_p = \arctan\left(\frac{f_c \sin \phi_c \sin \theta_c - u_p \cos \phi_c - v_p \sin \phi_c \cos \theta_c}{f_c \cos \phi_c \sin \theta_c + u_p \sin \phi_c - v_p \cos \phi_c \cos \theta_c}\right)$$

$$\gamma_p = \arccos(\cos(\theta_s) \cos(\theta_p) + \sin(\theta_s) \sin(\theta_p) \cos(\phi_p - \phi_s))$$

u_p and v_p are the pixel coordinates of a point p and f_c is the focal length of the camera. θ_p and ϕ_p are the corresponding zenith and azimuth angles and γ_p is the relative orientation to solar position. By substituting for these and the parameters a, b, c, d, e in equation 2 we rewrite f in terms of the variables of interest to our problem, as g . We have,

$$L(\theta_p, \gamma_p) = L_0 \frac{g(\theta_c, \phi_c, u_p, v_p, t)}{g(0, \phi_s, 0, 0, t)} \quad (3)$$

4.2 Radiometric Calibration

Digital cameras are not designed to capture the entire radiance range in the real world. The camera applies a non-linear mapping called the *response function* to the scene radiance to generate a smaller, fixed, range of image intensity values. In order to measure scene radiance from image intensities, it is necessary to learn the inverse response function. This is called radiometric calibration. A common approach is to take a series of images with varying camera exposures settings and estimate the inverse response function. This is not feasible for our application because we cannot control the

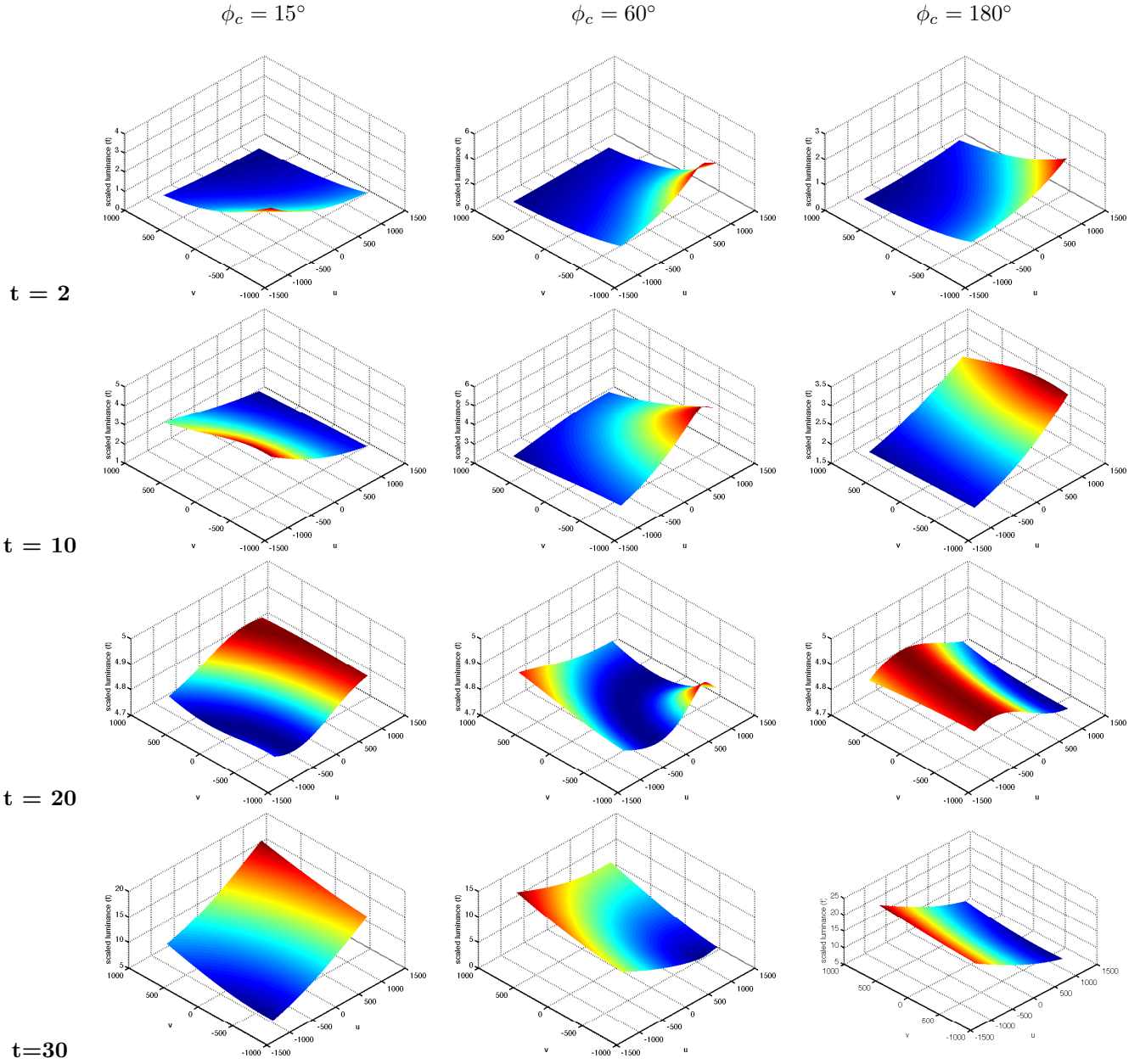


Figure 8: Illustration of the Perez model for sky luminance. The luminance ratio (f) changes significantly with turbidity. In the above graphs $f_c = 2031$ (based on HTC G1 phone camera), $\theta_c = 45^\circ$, $\theta_s = 30^\circ$ and $\phi_s = 0$. Note that the scale of the z axis is different for different graphs. In general, the luminance ratio increases as the turbidity increases.

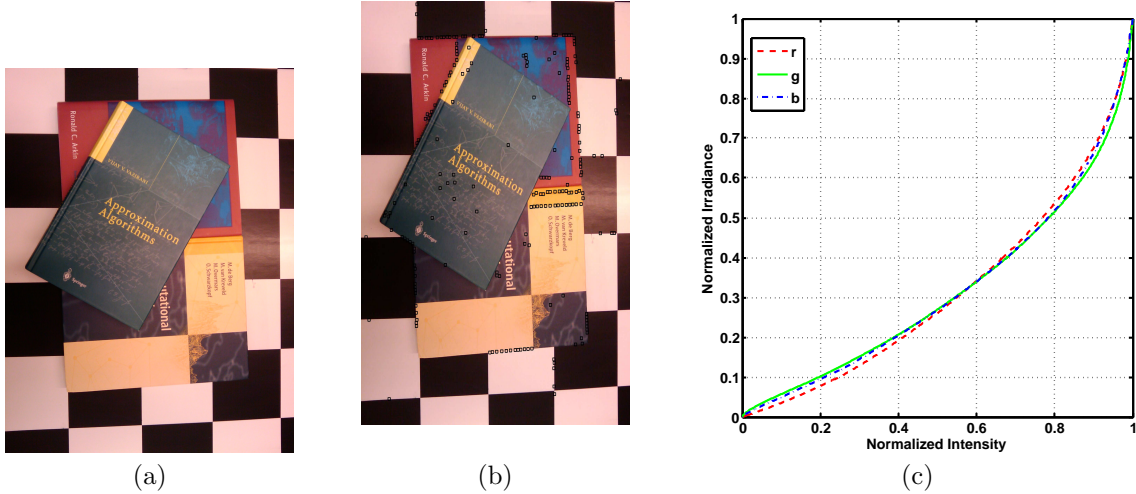


Figure 9: (a) image (b) corners used for estimation (c) resulting response functions for red, blue, green channels

exposure settings on most phones. We use the technique proposed by Lin et al [10] that uses a single image as suggested in [9].

The method works by first extracting color edges in an image and finding an inverse response function that results in an almost linear color blending in RGB space. This is done using *maximum a posteriori* estimation where the probability of an inverse response curve is proportional to the distance in RGB space between edge colors and prior model is obtained from [6]. Both the image intensity and irradiance values are normalized to [0 1]. Figure 9 shows the resulting curves for red, green and blue channels for the HTC G1 phone obtained by calibrating over 10 different images and 3 different phones.

4.3 Visibility Estimation

Visibility is estimated by matching the scaled luminance ratio (f) with the observed image intensity values at sky pixels after the radiometric calibration. Intensity I is computed from RGB values using the CIE standard formula $I = 0.2126R + 0.7152G + 0.0722B$. We find the value of t that minimizes the sum of squared error between measured intensity and the analytic luminance value over the set P of sky pixels.

$$(t, k) = \underset{t, k}{\operatorname{argmin}} \sum_{p \in P} \left(I_p - kg(\theta_c, \phi_c, u_p, v_p, t) \right)^2$$

The scaled luminance ratio g is computed using the solar position, camera orientation, and focal length data reported by the phone. Note that we cannot recover true irradiance values from the image but only scaled values. The Perez model for g also captures the luminance ratio with respect to the zenith. Therefore there is a constant factor k between the image intensity I and f at each pixel which can be estimated.

The above optimization can be solved using standard techniques such as Levenberg-Marquardt. We use initial values of 2 for t and 0.5 for k and bounds of [0 40] for t and [0 1] for k .

In our experiments, we observed that the compass on the phone gives a significant error. Therefore, we modify the optimization to estimate compass offset $\Delta\phi_c$.

$$t = \underset{t, k, \Delta\phi_c}{\operatorname{argmin}} \sum_p \left(I_p - kg(\theta_c, \phi_c + \Delta\phi_c, u_p, v_p, t) \right)^2 \quad (4)$$

5. EXPERIMENTS

This section describes a series of experiments conducted to validate our system and study its sensitivity to error in sensor data. We conducted two sets of experiments. The first on static camera setups used to monitor weather and visibility conditions. These images do not have significant orientation error and allow us to study the system on a series of images of the same scene. The second set of images are taken from the HTC G1 mobile phone using the visibility application described above. In all these experiments, the complete image was logged and the sky part was segmented interactively at the backend during processing.

5.1 Static camera image sources

South Mountain Web Camera

The Arizona Department of Environmental Quality (ADEQ) maintains several cameras near Phoenix. We used images from a 2.4 megapixel camera located in the North Mountains looking south. The pictures from this camera are published every 15 minutes. We used the method in [9] to calibrate the focal length and the azimuth and zenith angles of this

camera.

Altadena Weather Station

This 5 megapixel camera located in Altadena in California looks north-northeast towards the San Gabriel valley. It takes a picture every 5 minutes that is published online. Again, we use [9] to calibrate the camera.

USC Rooftop Camera Station

Recently, we set up an image station on the roof of a building at the University of Southern California (figure 11). It has an android phone placed inside a weather-proof box. It looks northeast at the Los Angeles downtown and logs images every 15 minutes. The focal length of the camera was estimated using the MATLAB calibration toolbox [3].

Results

Figure 10 shows three examples of images from the South Mountain camera that are reported to have good, fair and poor visibility by the ADEQ. The corresponding image intensity surfaces and the scaled luminance profiles for the values of turbidity (2, 3 and 6) estimated by our algorithm are shown. The turbidity values increase as the visibility decreases and the luminance surfaces match well with the image intensity profiles.

For the camera in Altadena, there is no ground truth visibility data available. Therefore, instead of comparing visibility values, we look at the average trend in visibility during a day (figure 12) averaged over 50 days during March 2009 to July 2009 (we eliminated days that had cloudy skies). The turbidity values are highest around 9 am and then steadily decrease to reach a minimum around 4 pm. This is in fact a well known trend in particulate matter concentration. As an example, we plot the PM2.5 concentration in central Los Angeles over the same 50 days

5.2 HTC G1 Phone

The HTC G1 phone was used to gather data using our application in the Los Angeles basin. The data was gathered over a period of 3 months. We focus on 3 significant visibility events during this time when the Air Quality Index (AQI) published by the South Coast Air Quality Management District (AQMD) had extreme values. 1) *fire day*: the Los Angeles wildfires around August 26th 2009 when the AQI was 150 and labeled 'unhealthy' 2) *hazy day*: an extreme low air quality day on November 8th 2009 when the AQI was 120 and labeled 'unhealthy for sensitive groups' and 3) *clear day*: an extreme clear air quality day following rain and snow on December 8th 2009 when the AQI was 23 and labeled 'good'. Figure 13 shows two representative images for each of the clear day and fire day and the luminance profiles for turbidity values of 2, 10, and 11. We also show the variation in error for different values of t . For the fire day, the intensity surface has a different shape compared to the analytic model. We believe this is because of inhomogene-

ity in the atmosphere caused by uneven clouds of smoke. The images shown here are facing the Los Angeles National Forest where the fires took place. Because the surfaces do not match properly, increasing t from 5 to around 17 also has very little impact on error.

5.3 Sensitivity analysis of camera orientation error

We conducted a series of experiments to study the error in the HTC G1 phone's orientation sensing and its impact on estimated luminance values. To compute the error, we captured images of the sun using our visibility application and calculated the solar position in the image using the time of day, GPS, and camera orientation reported by the phone. We then compared these pixel coordinates with visually detected solar position in each image (figure 16(a)). The resulting error over 100 images taken using 8 different phones is shown in figure 16(b) and (c) for azimuth and zenith angles. While the zenith error is mostly within $\pm 5^\circ$, the azimuth error is significantly larger.

We analyzed the impact of error on the azimuth angle on the intensity ratio. Figure 15 shows the derivative of luminance ratio $f(\theta_p, \gamma_p)$ with respect to camera azimuth ϕ_c for different values of solar zenith. The solar azimuth, ϕ_s , is fixed at 0° and the camera zenith, θ_c , is fixed at 45° . Repeating the computation for different values of ϕ_s and θ_c produces similar graphs. The graph shows that for ϕ_c between 100° and 160° , the luminance ratio varies only slightly with ϕ_c .

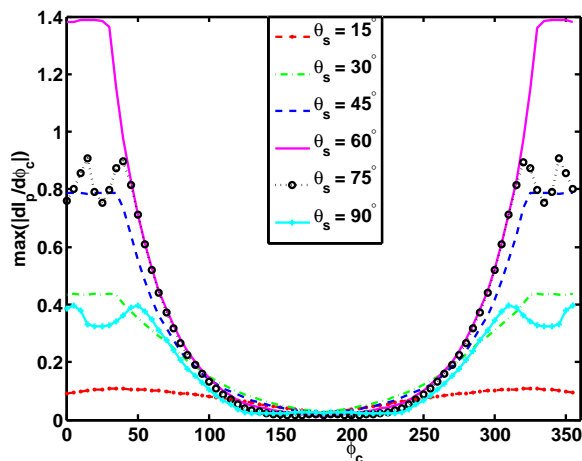
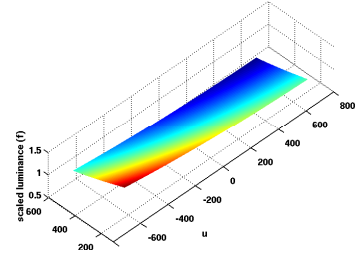
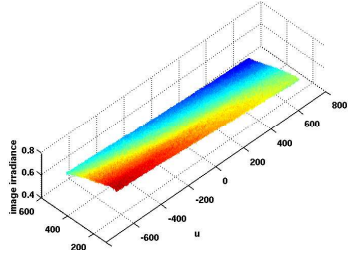


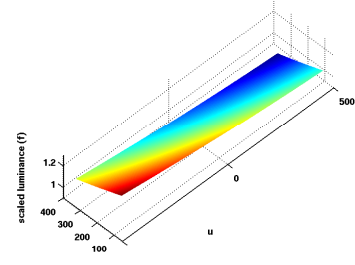
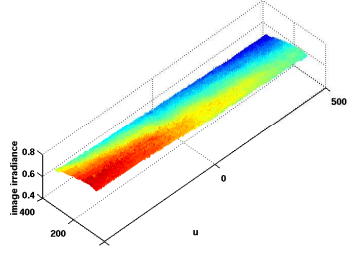
Figure 15: Sensitivity of luminance to compass error

5.4 Localization

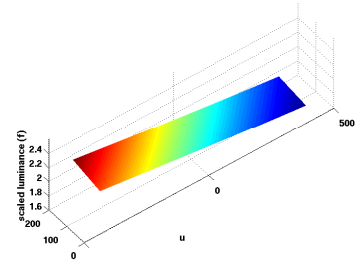
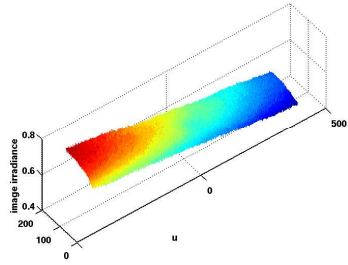
The GPS data is used to calculate the positions of sun. However, the position of sun changes very slowly with location. For instance, in Los Angeles (latitude $34^\circ N$ and longitude $118^\circ W$ the solar azimuth changes by less than a



Good visibility, $t = 2$



Fair visibility, $t = 3$



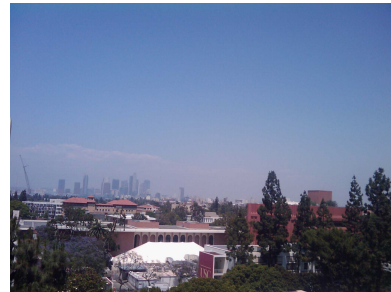
Poor visibility, $t = 6$

(a) Image

(b) Intensity

(c) model luminance

Figure 10: Results from the South Mountain Camera



(a)

(b)

(c)

Figure 11: USC Rooftop Camera Station

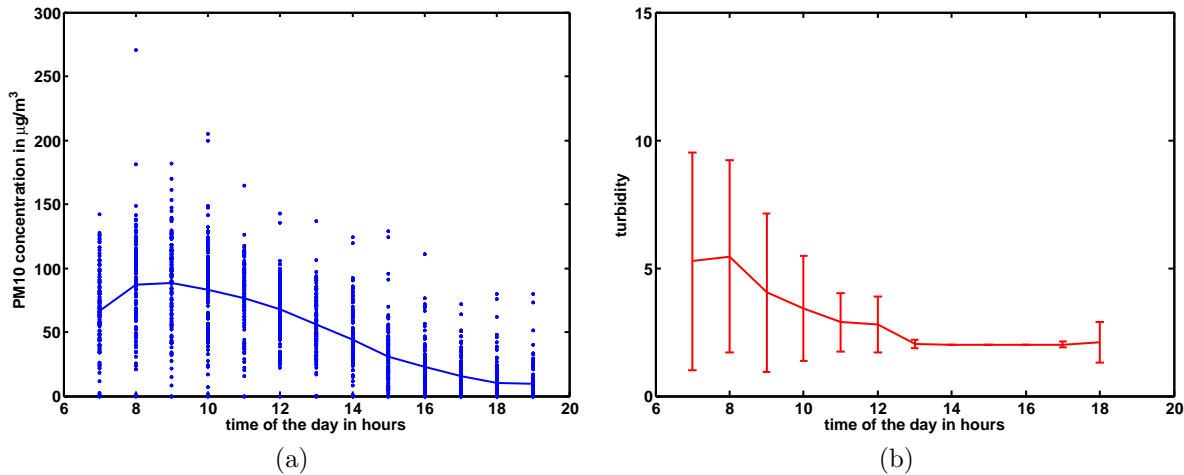


Figure 12: (a) Scatter plot of pollution data during a single day averaged over 50 days in central Los Angeles. (b) Average visibility data estimated using images over 50 days from a camera in Altadena

degree for over 60 miles. Therefore, a city-level localization can compute the solar position accurately enough. The sensitivity of luminance to solar azimuth is exactly the same as camera azimuth because the model only uses relative azimuth angle.

6. RELATED WORK

In this section we review current research in three areas related to our work.

Image processing based visibility mapping: There is a growing interest in monitoring environmental conditions using commodity cameras. Several approaches have been proposed to compute visibility from images. In [17], visibility is computed as the ratio of pixel contrast just below and just above the horizon. The method relies on being able to detect the horizon accurately which is challenging especially in poor visibility conditions. It is well suited for static web cameras where the horizon does not change and therefore can be computed on a clear day. Another approach is to use Fourier analysis of the image since clear images are likely to have more high frequency components ???. This approach applies to cases where the objects in the image are at a similar distance away as the visibility range. Other methods such as [2] and [15] require detection of a large number of visual targets either manually or automatically. All the above methods are based on image processing alone. In contrast, the approach we propose is based on an analytic model of sky appearance that takes into account the camera’s orientation and solar position.

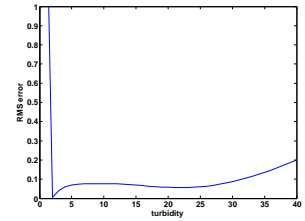
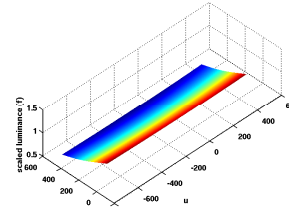
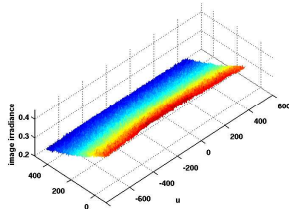
Air quality mapping using phones: Owing to the ubiquity of mobile phones, researchers have proposed integrating chemical sensors with mobile phones to measure air quality [5, 7] thus allowing large-scale sensing. Our work is in the same spirit of participatory sensing but we seek to measure air quality using sensors commonly available on phones.

Sky model based camera calibration: Models of sky appearance have been studied for several years and the computer graphics community has used these models for realistic rendering for scenes. In the past few years, these models have been used to analyze images to study photometric properties of scenes [18]. Recently, Lalonde et al, have calibrated the focal lengths and orientations of a large number of web cameras using images available on the internet [9]. We use the same approach to estimate visibility. The key difference in our case is that unlike web cameras, the camera in our case can be controlled and its geometric parameters are known.

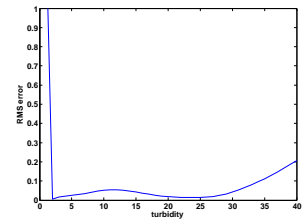
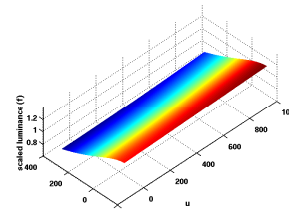
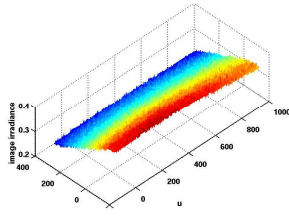
7. CONCLUSION

Air quality is a serious global concern that affects our health as well as the environment. While several efforts are underway to monitor and disseminate air quality information, the sensing locations are still extremely sparse because the monitoring stations are expensive and require careful installation and maintenance. Our vision is to augment these precise but sparse air quality measurements with coarse, large-scale sensing using commodity sensors. To this end, we propose a system that uses cameras and other sensors commonly available on phones to estimate air visibility. Using accelerometer and magnetometer data along with coarse location information, we generate an analytic model for sky appearance as a function of visibility. By comparing this model with an image taken using the phone, visibility is estimated. We present the design, implementation and evaluation of the system on the HTC G1 phone running Android OS with a backend server. To ensure user privacy, GPS data is processed on the phone and the image is cropped to contain only sky pixels before sharing it with the server. Our results show that the system can reliably distinguish between clear and hazy days.

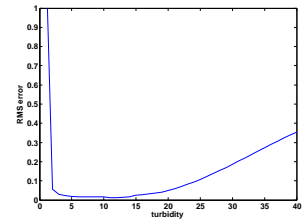
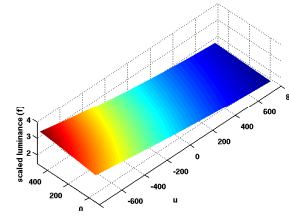
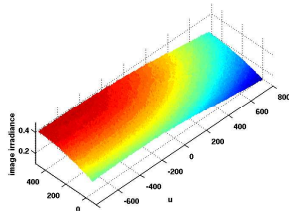
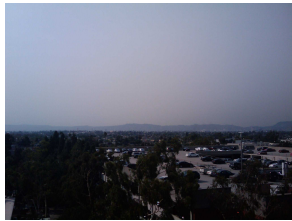
While our initial results are promising, several challenges



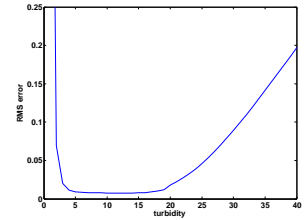
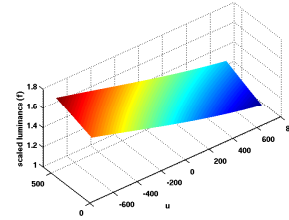
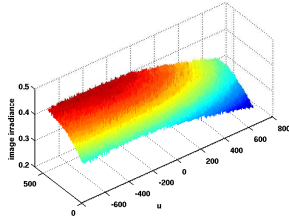
Clear day, $t = 2$, AQI 23



Clear day, $t = 2$, AQI 23

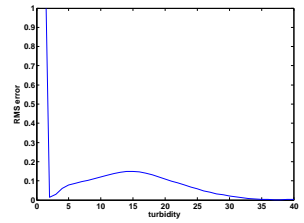
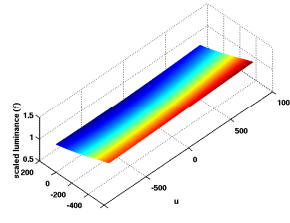
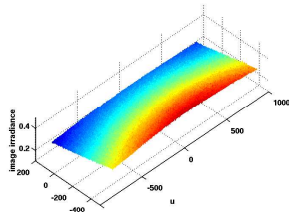


LA wildfires day, $t = 11$, AQI 150

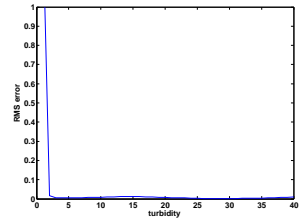
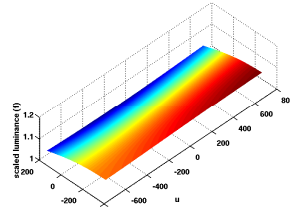
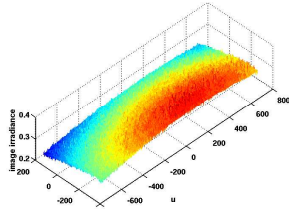


LA wildfires day, $t = 10$, AQI 150

Figure 13: Comparison of images taken during wildfires in Los Angeles on 30th August 2009 with those taken on a very clear day on 8th December 2009

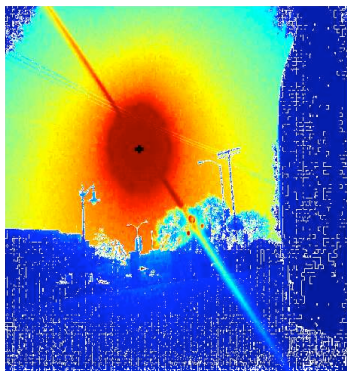


Clear day, $t = 2$, AQI 23

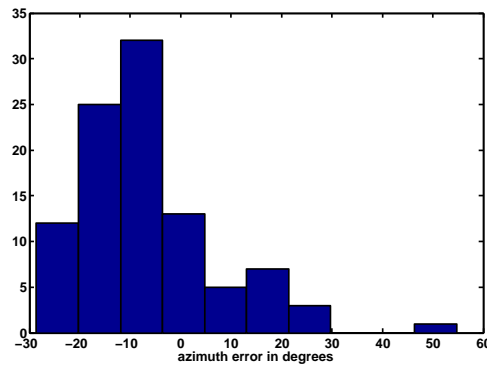


Hazy day, $t = 9$, AQI 120

Figure 14: Comparison of images taken during a hazy day on 8th November 2009 with those taken on a very clear day on 8th December 2009. In this case, the pictures were taken at the same time of the day 3pm



(a)



(b)

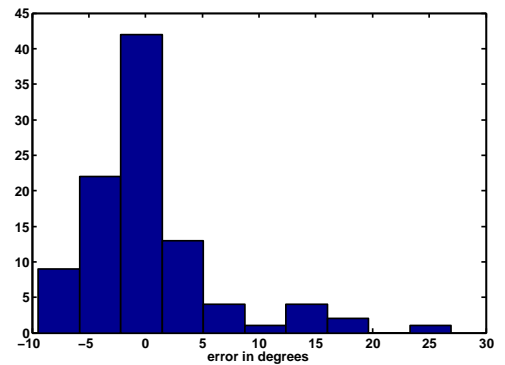


Figure 16: Compass error in HTC G1 phones

exist. First, the model assumes that the atmosphere is homogenous. This is generally true in the horizontal direction but when looking at an angle the haze tends to be layered. The impact of this is clear in the images we took during wildfires in Los Angeles. To address this we plan to investigate further sky models and also use the sensors on the phone to guide the user to gather data at favorable angles. Second, we currently assume that after the user crops the image, it does not have any clouds. While cloudy skies are a fundamental limitation of this approach, we plan to develop segmentation techniques that will allow us to use disconnected cloud-free sky segments.

Acknowledgements

We thank Bill Westphal and the Arizona Department of Environmental Quality for sharing the Altadena web camera data and the Phoenix South Mountain camera data respectively.

8. REFERENCES

- [1] U. E. P. Agency. Visibility in mandatory federal class I areas, 1994-1998 a report to congress, 2001.
- [2] D. Baumer, S. Versick, and B. Vogel. Determination of the visibility using a digital panorama camera. *Atmospheric Environment*, 42(11):2593–2602, 2008.
- [3] J.-Y. Bouguet. Camera calibration toolbox for matlab, 2008.
- [4] D. Dockery, C. Pope, X. Xu, J. Spengler, J. Ware, M. Fay, B. Ferris, and F. Speizer. An association between air pollution and mortality in six US cities. *The New England journal of medicine*, 329(24):1753, 1993.
- [5] P. Dutta, P. Aoki, N. Kumar, A. Mainwaring, C. Myers, W. Willett, and A. Woodruff. Common Sense: participatory urban sensing using a network of handheld air quality monitors. In *Proceedings of the 7th ACM Conference on Embedded Networked Sensor Systems*, pages 349–350. ACM, 2009.
- [6] M. Grossberg and S. Nayar. What is the space of camera response functions? In *IEEE Computer Society conference on Computer Vision and Pattern Recognition (CVPR)*, volume 2. Citeseer, 2003.
- [7] R. Honicky, E. Brewer, E. Paulos, and R. White. N-smarts: networked suite of mobile atmospheric real-time sensors. In *Proceedings of the second ACM SIGCOMM workshop on Networked systems for developing regions*, pages 25–30. ACM, 2008.
- [8] P. Ineichen, B. Molineaux, and R. Perez. Sky luminance data validation: comparison of seven models with four data banks. *Solar Energy*, 52(4):337–346, 1994.
- [9] J.-F. Lalonde, S. G. Narasimhan, and A. A. Efros. What do the sun and the sky tell us about the camera? *In submission, International Journal on Computer Vision*, 2009.
- [10] S. Lin, J. Gu, S. Yamazaki, and H. Shum. Radiometric calibration from a single image. In *Computer Vision and Pattern Recognition, 2004. CVPR 2004. Proceedings of the 2004 IEEE Computer Society Conference on*, volume 2, 2004.
- [11] E. McCartney. *Optics of the Atmosphere: Scattering by molecules and particles*. John Wiley, New York, 1976.
- [12] R. Perez, R. Seals, and J. Michalsky. All-weather model for sky luminance distribution. Preliminary configuration and validation. *Solar Energy*, 50(3):235–245, 1993.
- [13] K. Prather. Our Current Understanding of the Impact of Aerosols on Climate Change. *ChemSusChem*, 2(5), 2009.
- [14] A. Preetham, P. Shirley, and B. Smits. A practical analytic model for daylight. In *Proceedings of the 26th annual conference on Computer graphics and interactive techniques*, pages 91–100. ACM Press/Addison-Wesley Publishing Co. New York, NY, USA, 1999.
- [15] D. Raina, N. Parks, W. Li, R. Gray, and S. Dattner. An Innovative Methodology for Analyzing Digital Visibility Images in an Urban Environment. *Journal of the Air & Waste Management Association*, 55(11):1733–1742, 2005.
- [16] I. Reda and A. Andreas. Solar position algorithm for solar radiation applications. *Solar Energy*, 76(5):577–589, 2004.
- [17] L. Xie, A. Chiu, and S. Newsam. Estimating Atmospheric Visibility Using General-Purpose Cameras. In *Proceedings of the 4th International Symposium on Advances in Visual Computing, Part II*, page 367. Springer, 2008.
- [18] Y. Yu and J. Malik. Recovering photometric properties of architectural scenes from photographs. In *SIGGRAPH '98: Proceedings of the 25th annual conference on Computer graphics and interactive techniques*, pages 207–217, New York, NY, USA, 1998. ACM.